Shakil, Saani; Lu, Wei; Puttonen, Jari

Experimental studies on mechanical properties of S700 MC steel at elevated temperatures

Published in:
Fire Safety Journal

DOI:
10.1016/j.firesaf.2020.103157

Published: 01/09/2020

Document Version
Publisher's PDF, also known as Version of record

Fire Safety Journal 116 (2020) 103157

Contents lists available at ScienceDirect

Fire Safety Journal

journal homepage: http://www.elsevier.com/locate/firesaf

Experimental studies on mechanical properties of S700 MC steel at elevated temperatures

Saani Shakil *, Wei Lu, Jari Puttonen

Aalto University, Department of Civil Engineering, Finland

ARTICLE INFO

Keywords:
High strength steel
Mechanical properties at elevated temperatures
Transient state and steady state tests
Material modelling
Structural fire design

ABSTRACT

At elevated temperatures, the mechanical properties of high strength steel (HSS) reported in the literature have an observable scatter. They differ from design code values that are mainly based on experiments on mild steel. In this paper, the mechanical properties of S700 MC at elevated temperatures were investigated with steady state and transient state tensile tests. The reduction factors of yield strength started to decrease from 100 °C onwards, while the EN 1993-1-2 values have no decrease up to 400 °C. The reduction factors of proportional limit were below the code values up to 200 °C. The modulus of elasticity was consistent when using both monotonic and repeated loading but differed from the code values. Further comparisons of the mechanical properties of steels with the same strength grade with the values in the literature confirm the importance of testing HSSs produced with different manufacturing processes. The constitutive equations and representative material models proposed for S700 MC also support the implementation of a performance-based approach to structural fire safety design.

1. Introduction

The loss of structural stability in steel frame buildings during fire exposure has resulted in economic losses, human casualties, and environmental pollution [1,2]. Such catastrophic incidents have prompted researchers to move from the traditional prescriptive design to a performance-based structural fire safety design (PBSFSD). A thorough understanding of the properties of construction materials such as steel at elevated temperatures is essential for the successful implementation of PBSFSD. The constitutive equations derived from the material properties, measured with standard tests, can improve the accuracy of material modelling and the reliability of structural simulations [3–5].

Structures built with high strength steel (HSS) have a high strength-to-weight ratio and can have longer spans than structures built with mild steel. These structural changes affect the exposure of the structural members to fire, which may alter structural behaviour. In order to accelerate the transition to the PBSFSD approach, material properties of HSS at elevated temperatures are needed to increase the reliability of material modelling. Studies on steels having a yield strength close to 700 N/mm^2 [6–14] point out that reduction factors for mechanical properties differ from the values provided in design standards like EN 1993-1-2 [15]. This is especially true for the modulus of elasticity. These variations indicate that the reduction factors provided in design standards like EN 1993-1-2 ought to be calibrated or updated when defining the material properties for different HSSs.

Since reduction factors in current design standards are based on tests performed with mild steel, a safe model for reduction factors of HSS material can be recommended only after analysing more experimental data [16]. Using different test methods, studies were carried out on steels with yield strength of 700 N/mm^2 having different chemical compositions and manufacturing processes. Neuenschwander et al. [9] performed steady state tests for S690QL. Using both steady state and transient state methods, Qiang et al. [11] tested S690QL—a quenched and tempered steel. Studies by Du et al. [8] on QT-S690 and TMCP-S690 steel indicated that at elevated temperatures, mechanical properties depend on the manufacturing process. In addition, the steel's chemical composition, especially the percentage of carbon, can further influence its mechanical properties at elevated temperatures. Chemical compositions have varied in comparative tests on HSSs presented in the literature. Maraveas et al. [16] pointed out that the mechanical properties of HSSs at elevated temperatures vary significantly, and they recommend further testing. The authors in Ref. [17] pointed out that, in the literature, values for the modulus of elasticity vary remarkably and discussed the implications for material modelling. Since elastic modulus was not measured in previous tests on S700QL [6], S700MC steel was selected for this study. Using this steel grade, detailed experimental tests were

* Corresponding author.
E-mail addresses: saani.shakil@aalto.fi (S. Shakil), wei.2.lu@aalto.fi (W. Lu), jari.puttonen@aalto.fi (J. Puttonen).

https://doi.org/10.1016/j.firesaf.2020.103157
Received 23 July 2019; Received in revised form 25 May 2020; Accepted 31 May 2020
Available online 30 July 2020

performed for determining its mechanical properties at elevated temperatures.

This paper presents the results of steady state and transient state tests on the mechanical properties of S700MC steel. Stress-strain curves are used to define mechanical properties such as yield strength, elastic modulus, ultimate tensile strength, and proportional limit. The results are compared with those found in the literature, including the values provided in EN 1993-1-2. Subsequently, new models for both mechanical properties and constitutive equations of materials are proposed by modifying those presented in EN 1993-1-2.

2. Materials and methods

2.1. Test specimens

The specimens were manufactured from a 4 mm steel sheet made of S700MC (hereafter, 'S700'). The steel was thermomechanically rolled for cold-forming. The chemical composition of the steel is shown in Table 1. The steel sheet fulfilled the requirements according to EN 10051 [18] and EN 10149-2 [19]. The tensile specimens were dimensioned according to recommendations in EN ISO 6892-2 [20]. A water jet cutter was used to manufacture the specimens. Compared to the machining process, the water jet cutting technique offered higher cutting precision without localised heating. In terms of thickness, the dimensions of the opposing faces of the specimens were slightly different due to the profile of the water jet; however, since the differences were small, the dimensions of the specimens were deemed acceptable for tensile tests. The final dimensions of the specimens are shown in Fig. 1.

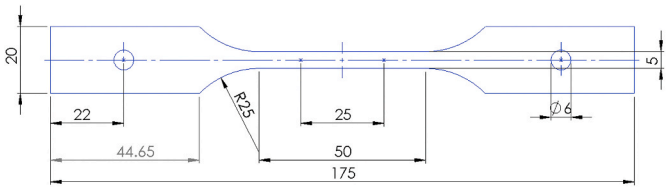

Fig. 1. Test specimens (units in mm).

2.2. Test setup and procedure

The overview of the test arrangement is shown in Fig. 2 (a). The specimens were tested inside a furnace manufactured by Maytec GmbH. The furnace was retrofitted to a tensile testing machine manufactured by Roell+Korthaus GmbH with a load range of 0–50 kN. The temperature of the furnace was controlled with a separate controlling unit connected to three temperature-detecting elements inside the furnace. The temperatures of the steel specimens were measured using Type K thermocouples at three locations along the parallel length of the specimens, as shown in Fig. 2(c). The measured steel temperature with respect to the furnace temperature was used to interpret the results of the loading tests. To protect the load cell located above the furnace, the specimens were fixed by a longer upper clamp rod.

The strain was measured with an extensometer with two ceramic rods, as shown in Fig. 2(b). The extensometer had a gauge length of 25 mm and could measure up to 16% extension with an accuracy of ±0.003 mm. The tips of the extensometer's ceramic rods were positioned in the dents punched in the middle of the specimens. In order to ensure firm contact between the rods and the specimens, the dial of the extensometer was manually rotated with controlled pressure. As deformation was observed to speed up within the range of 5–6% at room temperature, the extensometer was removed at 6% extension to protect the fragile ceramic rods. In order to obtain a complete curve up to failure, the strain beyond 6% was measured using the crosshead movement of the tensile testing machine.

To measure the mechanical properties of S700, both steady state and transient state tests were conducted in accordance with EN ISO 6892-2 [20], which also increased the overall reliability of the measurements. For both types of tests, a pre-load of approximately 10% of the nominal yield strength at room temperature was applied to ensure that the setup was stable before attaching the extensometer. The steady state tests were performed at the following temperatures (°C): 200, 400, 500, 600, 700, and 800. For these tests, the temperature was raised to the specific levels at a rate of 20 °C/min and was then maintained at each level for 12 min. After that, the specimens were loaded with a strain rate of $0.00025s^{-1}$ until failure. The steady state tests also produced continuous stress-strain curves through which the mechanical properties can be determined directly. The transient state test represents the mechanical and thermal loading scenario of materials exposed to fire in typical buildings. Moreover, the reduction factors in EN 1993-1-2 are based on the results of transient state tests, as pointed out in Ref. [21]. These tests include the effects of creep implicitly. For these tests, the specimens were first loaded to a specified stress level, and then the temperature was raised at a rate of either 10 °C/min or 20 °C/min until they failed or the furnace reached a temperature of 900 °C. The following stress levels were used (N/mm^2): 15, 60, 90, 120, 180, 250, 320, 400, 500, 600, 700, 730, and 750.

According to a preliminary study [17], values for the modulus of elasticity vary more than yield strength when the results from different tests were compared. In order to ensure the reliability of results, another series of steady state tests at elevated temperatures was carried out to measure the modulus of elasticity. In this series, instead of loading up to failure, the specimens were unloaded at 2% of total strain. After the load level dropped to the initial pre-load value, the specimens were reloaded up to failure. A summary of the tests carried out in this study can be found in Table 2.

2.3. Determination of mechanical properties from the stress-strain curves

According to the recommendation in EN ISO 6892-1 [22], the modulus of elasticity can be calculated using the initial linear portion of the curve and the least squares method to fit the test data in the elastic range. Upon close examination of the stress-strain curves, the initial portion of the curves is prone to irregularity caused by the imperfect initial shape of the specimens and by the slip in the components of the testing system [9]. Moreover, especially for temperatures higher than 400 °C, the initial portion of the curves is highly non-linear. Therefore, regression analysis of the curves between the upper and lower stress values corresponding to 40% and 10% of yield strength was used to calculate the elastic modulus [22] (Fig. 3). The modulus of elasticity calculated using this method and based on the results from tensile tests under monotonic loading is labelled $\mathbf{E_L}$.

Based on the results of the repeated loading tests, three sets of modulus of elasticity was determined. Similar to the method mentioned above, the first set of values was calculated using the linear part of the loading curve ($\mathbf{E_L}$). The second set was calculated using the linear part of the reloading curve ($\mathbf{E_{HL}}$). In the third set, the secant modulus was calculated using the crossing point H2 and the lowest stress point H1 on the hysteresis curve, as shown in Fig. 3. This set of values for the elastic modulus is labelled $\mathbf{E_H}$.

Table 1
Chemical composition (%) of S700 MC steel.

C	Si	Mn	P	S	Al	Nb	V	Ti	Cu	Cr	Ni	Mo	B	Zr
0.056	0.18	1.78	0.01	0.003	0.038	0.06	0.01	0.116	0.011	0.04	0.03	0.005	0.0004	0.003

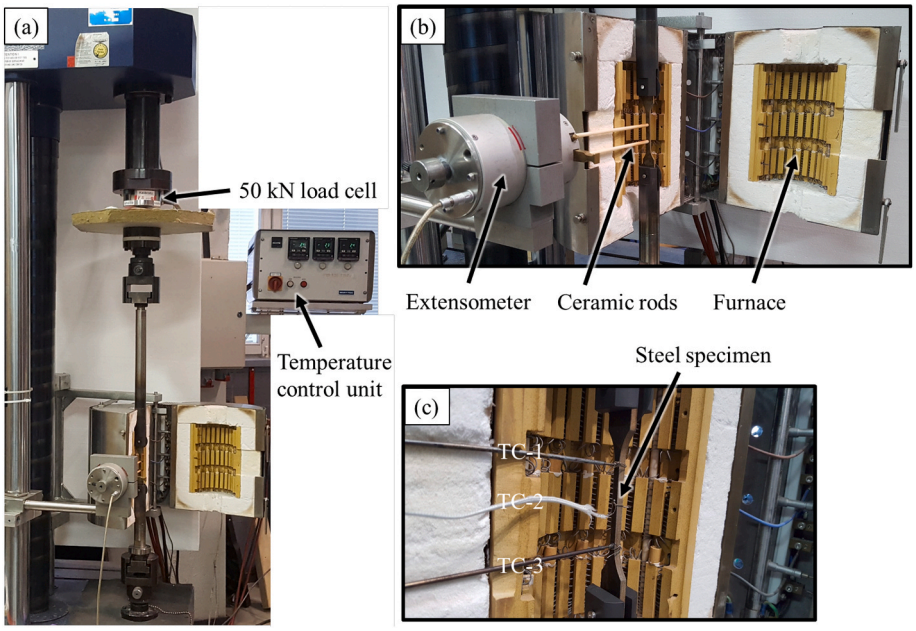

Fig. 2. Tensile testing and temperature measurement equipment: (a) overview of the test setup; (b) detailed setup for measuring the strains; and (c) detailed setup for measuring steel temperature (TC: thermocouple).

Table 2
Summary of tests performed in this research.

Type of test	Stress or temperature levels	Number of repetitions
Steady state (monotonic loading)	200, 400, 500, 600, 700, and 800 (°C)	2
Steady state (repeated loading)	same as previous row	1
Transient state at 10 °C/min	15, 60, 90, 120, 180, 250, 320, 400, 500, 600, 700, 730, and 750 (N/mm^2)	2
Transient state at 20 °C/min	same as previous row	1

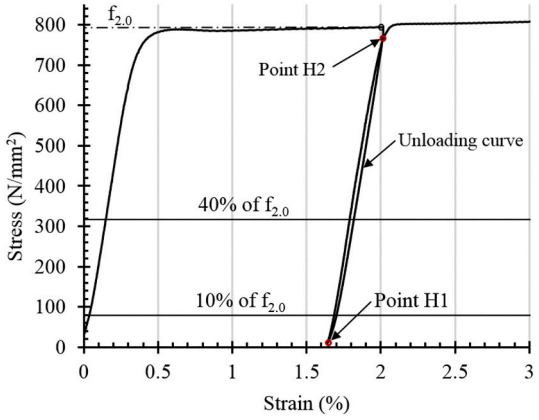

Fig. 3. Schematics for the evaluation of elastic modulus using the stress-strain curve.

The effective yield strength at elevated temperatures can be obtained from the stress-strain curves, as shown in Fig. 4. Since the stress-strain curves become increasingly non-linear at elevated temperatures, the effective yield strength can be defined at various strain values. In EN 1993-1-2 [15], the effective yield strength is defined as the strength at 2% total strain, i.e. $f_{2.0}$. As recommended in Ref. [9,23], other methods

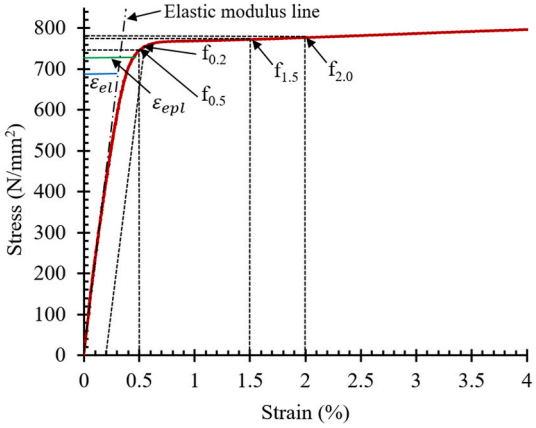

Fig. 4. Determination of effective yield strength and proportional limit based on the stress-strain curve.

for defining the effective yield strength are at 0.2% proof strength ($f_{0.2}$), and at total strains of 0.5% ($f_{0.5}$) and 1.5% ($f_{1.5}$).

The proportional limit marks the point on the stress-strain curve at which the stress ceases to be proportional to the strain. The pioneers of measuring the proportional limit, Rubert and Schaumann, pointed out that the proportional limit affects the stability of frames with high slenderness ratios at elevated temperatures [24]. Similar to the method used in Ref. [9], in this study, the proportional limit was defined as the stress at which the elastoplastic strain (ε_{epl}) on the stress-strain curve exceeds the strain of the elastic line (ε_{el}) by 2%, i.e. $\frac{\varepsilon_{epl}}{\varepsilon_{el}} \geq 1.02$, as shown in Fig. 4.

3. Mechanical properties determined from experimental tests

3.1. Mechanical properties at ambient temperature

In total, six tensile tests were carried out to find the mechanical properties of the material at ambient temperature. In accordance with the EN ISO 6892-1 [22] recommendation, the strain rate of $0.00025s^{-1}$

was used to obtain the whole range of stress-strain curve. The average values of the measured mechanical properties listed in Table 3 are modulus of elasticity ($E_{L,20}$), proportional limit ($f_{p,20}$), yield strength ($f_{0.2,20}$), ultimate tensile strength ($f_{u,20}$), strain at ultimate tensile strength ($\varepsilon_{u,20}$), and strain at fracture ($\varepsilon_{t,20}$). The proof strength at an offset of 0.2% was used to define the yield strength ($f_{0.2,20}$). The proportional limit was determined using the same procedure that was described in Section 2.3. The mechanical properties at room temperature are presented in Table 3 and, along with the results from the steady state and transient state tests, are used to calculate the reduction factors at elevated temperatures.

3.2. Stress-strain curves and mechanical properties from steady state tests

Fig. 5 shows the stress-strain curves obtained from steady state tests without unloading. These curves were taken from one of the two repetition tests. Fig. 5 shows that, similar to room temperature, the steel exhibits strain hardening at 200 °C but fails at a lower strain level. The effect of strain hardening diminished at 400 °C. At temperatures of 500 °C and above, specimen failure occurred well beyond 20% strain.

Fig. 6 shows the stress-strain curves obtained from steady state tests with unloading at a strain level of 2% and reloading up to failure. Hysteresis behaviour during the unloading and reloading process is apparent at all temperatures but is generally neglected in plasticity theories at room temperature. It can also be seen from the figure that the reloading part closely follows the trend of the initial loading part.

Using the stress-strain curves of steady state tests shown in Figs. 5 and 6, and another repetition test, the average values of mechanical properties were obtained and listed in Table 4; the corresponding reduction factors were calculated and listed in Table 5. As shown in Table 4, the effective yield strength defined at 2% strain was higher than the effective yield strengths defined at lower strains up to a temperature of 500 °C. When the reduction factors obtained for the respective yield strengths were compared to room temperature, the reduction of the effective yield strength was about 25% at 400 °C and 50% at 500 °C, as shown in Table 5.

In Table 4, $E_{L,\theta}$ is the average value of elastic modulus determined at temperature θ using the loading portion of the three stress-strain curves obtained from the monotonic and repeated loading tests. In Table 4, the values of $E_{L,s3,\theta}$ are determined from the initial loading part; $E_{HL,\theta}$ and $E_{H,\theta}$ are determined from the unloading-reloading part of the series 3 curve presented in Fig. 6. A comparison of the reduction factors of the elastic modulus determined using different criteria is also shown in Fig. 7(b). It can be seen from the table and the figure that up to a temperature of 400 °C, the values determined using different methods are quite similar. Beyond that, the elastic modulus shows a relatively larger scatter.

From the stress-strain curves shown in Fig. 6(b), the highly non-linear initial parts are observed above 400 °C. Additionally, clear hysteresis behaviour and high non-linearity are apparent at unloading and reloading portions at temperatures of 500 °C and above. The elastic modulus at higher temperatures is evidently sensitive to the test methods used [25], which can be attributed to creep and microstructure of the steel. The accuracy of any measurement method can be reserved until the validation of the material model is done using tests on the member level. The elastic moduli $E_{HL,\theta}$ and $E_{H,\theta}$ obtained in this study can be used to create a more precise material model that considers strain reversals due to mechanical unloading and reloading in the simulation.

Table 3
Average mechanical properties of the steel at room temperature.

Elastic modulus, $E_{L,20}$ (N/mm^2) × 10^3	Proportional limit, $f_{p,20}$ (N/mm^2)	Proof strength, $f_{0.2,20}$ (N/mm^2)	Ultimate tensile strength, $f_{u,20}$ (N/mm^2)	Strain at ultimate tensile strength, $\varepsilon_{u,20}$	Strain at fracture, $\varepsilon_{t,20}$
216	530	764	839	11.2%	15.1%

Table 4 also lists the values of proportional limit, which lie between 55% and 70% of the effective yield strength ($f_{0.2,\theta}$) at corresponding temperatures. The reduction factors for the proportional limit are presented in Table 5 and Fig. 7(a).

The maximum stress reached on the stress-strain curve is defined as the ultimate tensile strength, which is also used for elevated temperatures ($f_{u,\theta}$). Table 6 lists the values of the ultimate tensile strength ($f_{u,\theta}$), its comparison with the effective yield strength at 0.2% offset strain and 2% total strain, the strain corresponding to the ultimate tensile strength ($\varepsilon_{u,\theta}$), and the strain at fracture ($\varepsilon_{t,\theta}$). The reduction factors of the ultimate tensile strength defined as the ratio of $f_{u,\theta}/f_{u,20}$ are shown in both Table 6 and Fig. 7(a). From the ratio of $f_{u,\theta}/f_{0.2,\theta}$ in Table 6, it can be seen that the difference between the ultimate tensile strength and the effective yield strength ($f_{0.2,\theta}$) is smaller above 400 °C than at room temperature. This indicates that no significant strain hardening occurs above 400 °C. Compared to the ratio of $f_{u,\theta}/f_{0.2,\theta}$, the ratio of $f_{u,\theta}/f_{2,\theta}$ in Table 6 follows a similar trend but has slightly lower values at all temperatures except 700 °C. The strain at ultimate tensile strength ($\varepsilon_{u,\theta}$) is lower than the 2% total strain at 700 °C, which suggests that the necking starts earlier than 2% and, thus, using 0.2% offset strain to define the effective yield strength is more reasonable. However, further comparisons in Fig. 7(a) show that the reduction factors of ultimate tensile strength follow a similar trend and have values close to the reduction factors of yield strength measured at various strains. Therefore, by following the definition provided in EN 1993-1-2, the effective yield strength at 2% total strain is kept for further studies. However, redefining the effective yield strength for HSS could be a research topic worth exploring in the future. In general, the comparisons in Fig. 7 show that the yield strength and the modulus of elasticity deviate significantly from the values provided in EN 1993-1-2 between 200 °C and 800 °C, while proportional limit differs from the code values up to temperatures of 200 °C. Therefore, these properties were further examined in this study. Table 6 shows that, up to the temperature of 400 °C, the strain at fracture is in the range of 15.6%–17.5%, which is lower than the value of 20% provided in EN 1993-1-2. For temperatures of 500 °C and above, the value of the strain at fracture is more than 20%. Further research is necessary to redefine the maximum strain in the material models provided in EN 1993-1-2.

3.3. Stress-strain curves and mechanical properties from transient state tests

Fig. 8 shows the average values of both the furnace and the steel temperatures with respect to time for the two heating rates used (20 °C/min and 10 °C/min). As the temperature in the furnace increased, specimen temperature initially lagged behind the furnace temperature, but ultimately caught up and became equal to the furnace air temperature at around 500 °C. Beyond this point, the steel temperature was consistently slightly higher than the furnace air temperature. Since steel is a homogeneous material, the relationship between steel temperatures and the furnace temperatures is expected to be consistent with repetition tests. Therefore, steel temperatures were measured once and used together with furnace temperature to interpret the results of the transient tests.

The strain at elevated temperatures includes three components: the thermal strain, the stress-related strain, and the creep strain. Similar to EN 1993-1-2 [15], creep can be implicitly considered in the stress-strain relationships; therefore, only the thermal strain is excluded from the total strains. In Fig. 9, the thermal strains or elongations measured at a stress level of 5 N/mm^2 are compared with the values presented in Ref. [9,10] and EN 1993-1-2. It can be seen from the figure that the two heating rates result in somewhat similar curves for thermal elongation, which gradually start to deviate from the curve defined in EN 1993-1-2

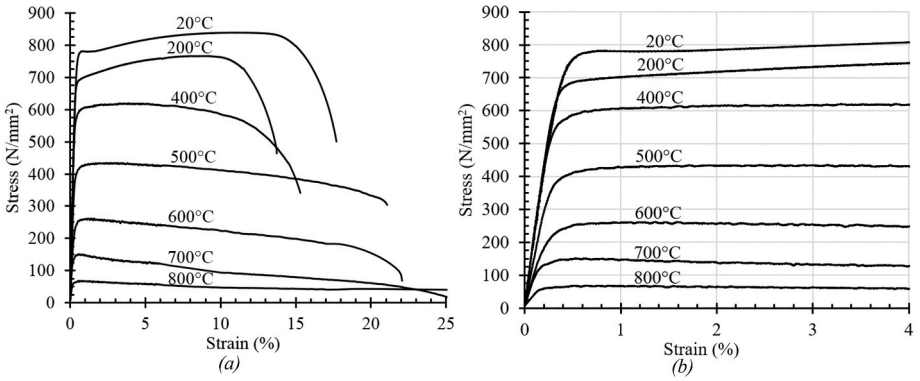

Fig. 5. Stress-strain curves obtained from steady state tests (series 1): (a) up to 25% strain; and (b) up to 4% strain.

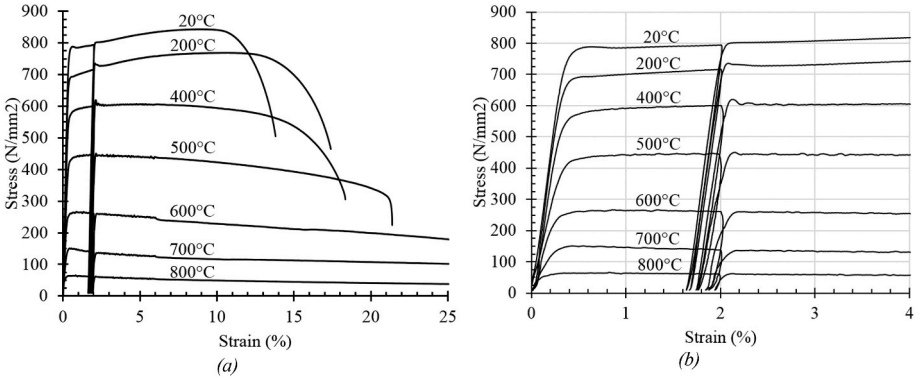

Fig. 6. Stress-strain curves obtained from steady-state tests (series 3) with unloading and reloading: (a) up to 25% strain; and (b) up to 4% strain.

Table 4
Effective yield strength, modulus of elasticity, and proportional limit determined from steady state tests.

Temperature (°C)	Effective yield strength (N/mm^2)				Modulus of elasticity (N/mm^2) × 10^3				Proportional limit (N/mm^2)
	$f_{0.2,\theta}$	$f_{0.5,\theta}$	$f_{1.5,\theta}$	$f_{2,\theta}$	Average of series 1, 2 and 3	Using series 3			$f_{p,\theta}$
					$E_{L,\theta}$	$E_{L,s3,\theta}$	$E_{HL,\theta}$	$E_{H,\theta}$	
20	764	759	781	785	216	216	214	200	530
200	691	690	712	720	223	216	216	200	456
400	576	578	603	606	208	202	203	187	366
500	415	415	433	435	135	127	158	144	294
600	247	250	261	257	109	112	151	133	138
700	145	148	141	137	89	73	110	80	83
800	63	65	62	63	46	62	50	60	46

Table 5
Reduction factors using steady state tests.

Temperature (°C)	Effective yield strength				Modulus of elasticity			Proportional limit
	$\frac{f_{0.2,\theta}}{f_{0.2,20}}$	$\frac{f_{0.5,\theta}}{f_{0.2,20}}$	$\frac{f_{1.5,\theta}}{f_{0.2,20}}$	$\frac{f_{2,\theta}}{f_{0.2,20}}$	$\frac{E_{L,\theta}}{E_{L,20}}$	$\frac{E_{HL,\theta}}{E_{HL,20}}$	$\frac{E_{H,\theta}}{E_{H,20}}$	$\frac{f_{p,\theta}}{f_{0.2,20}}$
20	1.000	0.994	1.022	1.028	1.000	1.000	1.000	0.694
200	0.904	0.903	0.932	0.942	1.035	1.007	1.000	0.597
400	0.754	0.757	0.789	0.794	0.966	0.949	0.935	0.479
500	0.543	0.543	0.566	0.569	0.627	0.736	0.700	0.385
600	0.323	0.327	0.341	0.337	0.509	0.653	0.625	0.181
700	0.190	0.193	0.184	0.180	0.415	0.515	0.400	0.109
800	0.082	0.085	0.082	0.082	0.213	0.232	0.300	0.060

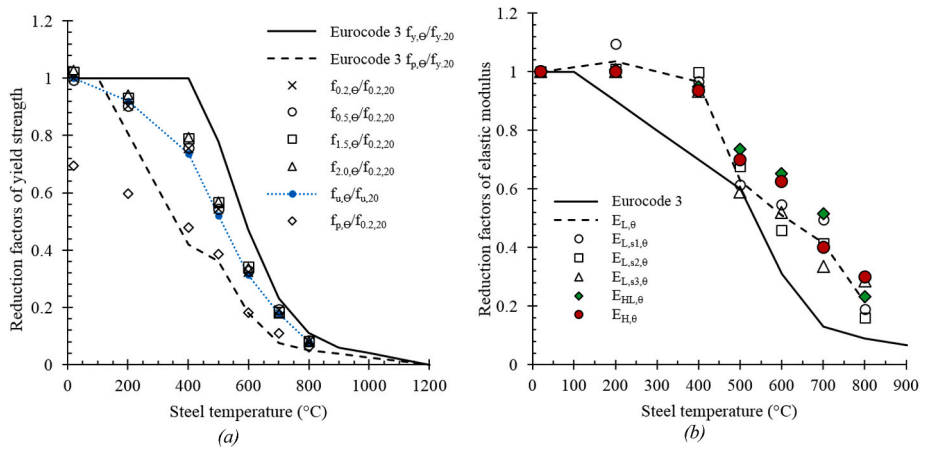

Fig. 7. Comparisons of measured mechanical properties defined using various criteria: (a) strength comparisons; and (b) modulus of elasticity (subscripts s1: series 1; s2: series2; and s3: series 3).

Table 6
Ultimate strength and the corresponding reduction factors.

Temperature (°C)	Ultimate tensile strength, $f_{u,\theta}$ (N/mm^2)	Strain at ultimate tensile strength, $\varepsilon_{u,\theta}$ (%)	Strain at fracture, $\varepsilon_{t,\theta}$ (%)	Reduction factors for ultimate tensile strength, $\frac{f_{u,\theta}}{f_{u,20}}$	Comparison to effective yield strength at the same temperature, $\frac{f_{u,\theta}}{f_{0.2,\theta}}$	Comparison to yield strength at the same temperature, $\frac{f_{u,\theta}}{f_{2,\theta}}$
20	839	11.2	17.5	1.000	1.10	1.07
200	771	9.8	15.6	0.919	1.12	1.07
400	618	3.3	17.1	0.736	1.07	1.02
500	437	2.7	21.0	0.521	1.05	1.00
600	262	1.2	23.6	0.313	1.06	1.02
700	150	0.6	23.9	0.178	1.03	1.09
800	66	1.0	25.0	0.079	1.05	1.05

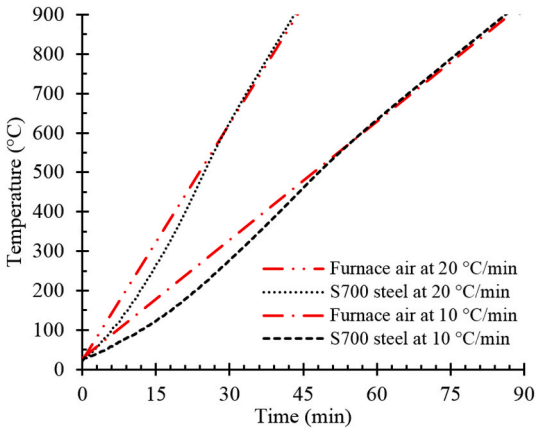

Fig. 8. Temperature development in the steel specimens along with the furnace at different heating rates.

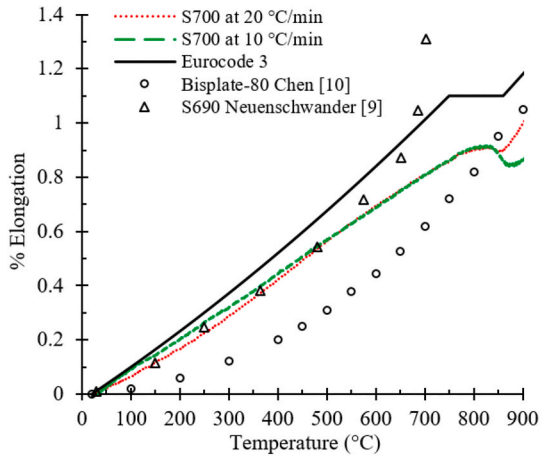

Fig. 9. Measured thermal elongation compared to EN 1993-1-2 and the literature values.

as the temperatures increase. According to EN 1993-1-2, thermal elongation remains constant between 750 °C and 860 °C because of the phase transformation of steel in this temperature range. Thermal elongation is apparently almost constant between the same temperature range of 750 °C and 860 °C when the heating rate is 20 °C/min; with a heating rate of 10 °C/min, the elongation decreases at 850 °C. When compared to the values of thermal elongation reported in the literature, the measured values are higher than those presented by Chen et al. [10] over the whole temperature range. The measured values are close to the values reported by Neuenschwander et al. [9] up to 550 °C, but are lower at temperatures higher than 550 °C. Further research is needed to explain the different trends in the values of thermal elongation in Fig. 9.

Fig. 10 shows the variation of the measured strains with temperature rise at different levels of stress. The stress-strain curves (Fig. 5) based on the steady state tests show that at the strain level of 6% the steel material is clearly in the plastic range; therefore, the tests were stopped at this strain. Fig. 10 shows that there is a dramatic strain variation within a short temperature range above the stress level of 700 N/mm^2. Below this stress level, the variation of strains depends more on the reduction of the modulus of elasticity and yielding develops gradually. Fig. 10 also shows the occurrence of runaway failure of the specimens at different highlighted stress levels corresponding to 0.5%, 1.5% and 2% strains. At 2% strain, the runaway failure can be clearly compared across the whole

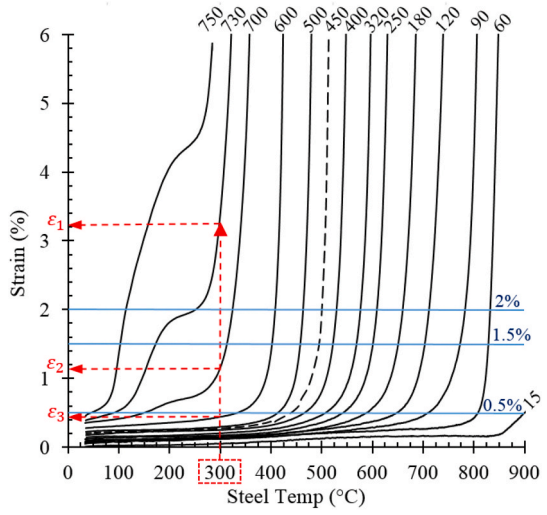

Fig. 10. Measured strain versus temperature curves for the specified stress levels (N/mm^2). The dashed line for 450 N/mm^2 is an example of the interpolated curves used for constructing Fig. 11.

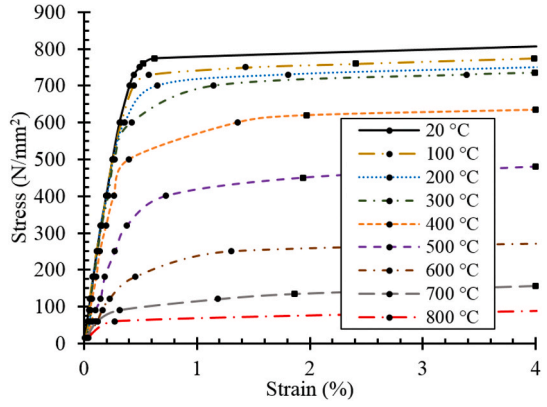

Fig. 11. Stress versus strain curves using transient state tests (up to 4% strain), where circles represent measured values and squares represent interpolated values.

range of stress levels.

Using the scheme highlighted at a temperature of 300 °C in Fig. 10, the measured strain-temperature curves were transformed to the stress-strain curves in Fig. 11. In order to complete the stress-strain curves in Fig. 11 up to the strain value of 4%, some missing points were taken from the interpolated curves of Fig. 10 (as in the case of 450 N/mm^2 curve). These interpolated points were marked as square markers in Fig. 11. Using these stress-strain curves, the mechanical properties similar to those in steady tests were obtained. The mechanical properties include the effective yield strength at different strain levels, the proportional limit, and the modulus of elasticity. The room temperature values in Table 3 were used to calculate the reduction factors using the transient state tests presented in Table 7. The effective yield strength based on 0.2% offset and 0.5% extension in transient tests was lower than the values in steady state tests by up to 10% at 400 °C and 500 °C, 20% at 600 °C, and 30% at 700 °C, but the effective yield strengths based on 1.5% and 2% extension was much closer. Fig. 10 affirms that the effective yield strength at 2% can be used to compare the results of the two types of tests.

Table 7
Reduction factors using transient state tests.

Temperature (°C)	Effective yield strength				Proportional limit	Modulus of elasticity
	$\frac{f_{0.2,\theta}}{f_{0.2,20}}$	$\frac{f_{0.5,\theta}}{f_{0.2,20}}$	$\frac{f_{1.5,\theta}}{f_{0.2,20}}$	$\frac{f_{2,\theta}}{f_{0.2,20}}$	$\frac{f_{p,\theta}}{f_{0.2,20}}$	$\frac{E_{L,\theta}}{E_{L,20}}$
20	1.000	0.988	1.008	1.014	0.694	1.000
100	0.955	0.942	0.982	0.991	0.668	1.035
200	0.877	0.864	0.949	0.957	0.654	1.011
300	0.815	0.800	0.929	0.941	0.622	0.916
400	0.681	0.674	0.798	0.812	0.524	0.875
500	0.510	0.478	0.575	0.589	0.380	0.508
600	0.257	0.249	0.340	0.353	0.170	0.383
700	0.126	0.131	0.170	0.177	0.118	0.309
800	0.080	0.085	0.096	0.102	0.072	0.170

3.4. Failure modes of the specimens

Failure modes of the steady state test specimens are given in Fig. 12, where the specimens are aligned so that the right side of the figure corresponds to the top clamp of the testing machine. The figure shows that the location of the necking as well as the failure of the specimen moved from the middle to the left as the temperature increased. However, the strain values for these cases were much greater than 6% at failure. Since the transient tests were stopped when either a strain of 6% or a furnace temperature of 900 °C was reached, failure was not achieved in these test specimens, as shown in Fig. 13. It can be seen from the figure that the specimen experienced uniform strain in the parallel length region.

4. Comparisons and discussion

In this section, the reduction factors of the mechanical properties based on the test results are compared with the reduction factors provided in EN 1993-1-2 and the literature. Using the reduction factors calculated in this study, equations were also derived, which were incorporated into the material models based on EN 1993-1-2 and Ramberg-Osgood formulations. The stress-strain curves of these material models are presented and compared with the test results.

4.1. Comparison of the reduction factors defined for mechanical properties

Fig. 14 shows the reduction factors of yield strength determined from both steady state and transient state tests with the values provided in EN 1993-1-2. As can be seen from the figure, reduction factors of yield strength were not significantly sensitive for the two heating rates. Fig. 14 also shows that the reduction factors of yield strength from both steady state and transient state tests lie close to each other throughout the temperature range. The reduction factors obtained from the tests follow trends similar to those in EN 1993-1-2, but between 200 °C and 700 °C the former values are lower than the latter values.

In Fig. 15, the reduction factors of yield strength calculated in this

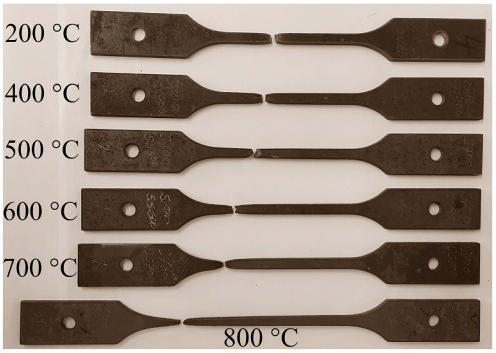

Fig. 12. Specimens after steady state tests.

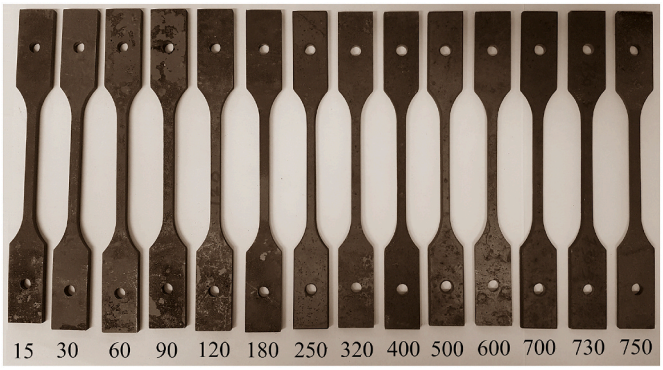

Fig. 13. Specimens after transient state tests at different stress levels (N/mm^2).

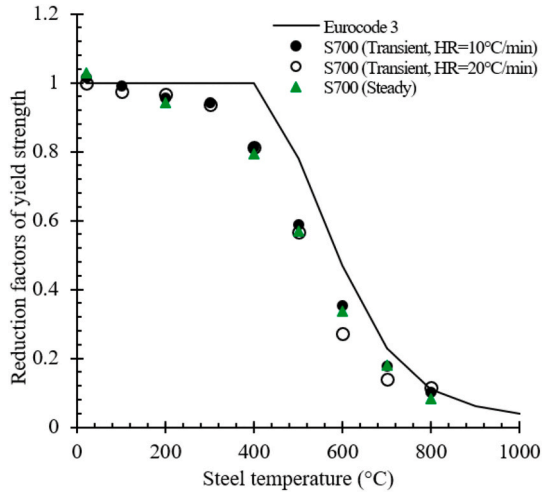

Fig. 14. Yield strength reduction factors of S700 compared to Eurocode 3 (HR: heating rate).

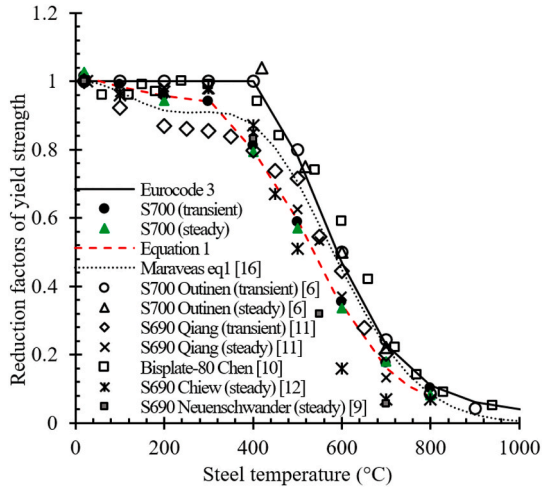

Fig. 15. Yield strength reduction factors of HSS compared to Eurocode 3 and other literature.

study are compared with those from the literature. It can be seen from the figure that the dispersion is clear among the values between temperatures of 200 °C and 700 °C. The reduction factors from this study are in the vicinity of the values from steady state tests by Qiang et al. [11]. Compared to the values from Chiew et al. [12], the current test values are higher from 450 °C onwards. The current test values are lower than the values provided by Chen [10] for the whole temperature range. Further comparisons show that the values of the current study are higher than those provided by Neuenschwander et al. [9] from 550 °C onwards. Fig. 15 also shows that the reduction factors provided in EN 1993-1-2 are larger than the majority of the results presented in the literature. In the tests carried out by Outinen et al. [6], the same equipment as in the current tests was used, but the specimen type and the manufacturing process of the same grade of steel were different. While Outinen et al. [6] used cylindrical specimens of S700 QL, the type of specimens in the current tests was flat and the steel grade was S700 MC. Besides the case-specific uncertainties of testing, the deviations between the results of the current test and the tests by Outinen et al. [6] are clearly caused by differences in chemical composition and the manufacturing processes of the steel.

Fig. 16 shows the reduction factors of the modulus of elasticity for steady state and transient state tests. It can be seen that the modulus of elasticity was not significantly sensitive for the two heating rates used in the transient state tests. The values obtained from transient state tests where creep is implicitly included were 10%–20% lower than those of steady state tests between 400 °C and 700 °C. In general, the values from steady state tests are higher than transient state tests.

Fig. 17 compares the reduction factors for the modulus of elasticity obtained in this study with results from other studies and EN 1993-1-2. Compared to the values provided in EN 1993-1-2, the reduction factors calculated from the current test results were higher, with the largest difference observed at 400 °C. The dispersion of the values is larger for temperatures over 200 °C. The values based on the current tests are similar to the values provided by Chiew et al. [12] and Neuenschwander et al. [9], and lie in between the values provided by Qiang et al. [11] and Chen et al. [10]. Fig. 17 indicates that the dispersion of the modulus of elasticity can be attributed to the test methods and conditions; it also shows that reduction factors in Eurocode 3 are smaller than most of the reduction factors reported.

In Fig. 18(a) and (b), the reduction factors for proportional limit obtained in this study are presented with those provided in EN 1993-1-2 and some other studies [9,26]. In Fig. 18(a), the values from the steady state and the transient state tests differ slightly only at 200 °C and 400 °C. Compared to the values in EN 1993-1-2, the proportional limit values found in this study are initially lower, but beyond 300 °C, the test values become similar to those in EN 1993-1-2. Fig. 18(b) shows that the values for the proportional limit are similar to the values presented in the references but with observable differences up to 400 °C. Based on the test results, the reduction factors of the proportional limit in the range of 20 °C–300 °C should be redefined in EN 1993-1-2 for the HSS studied.

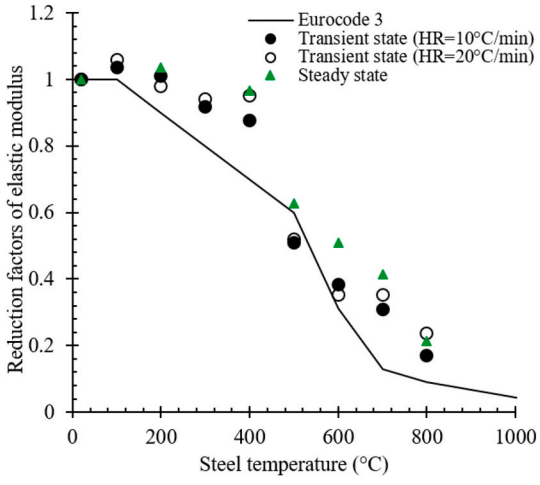

Fig. 16. Reduction Factors of Elastic modulus using ISO 6892-1 recommendation (HR: heating rate).

4.2. Prediction of the mechanical properties based on the test results

The studies in previous section show that the values of both yield strength and the proportional limit obtained from steady state and transient state tests were similar. The elastic modulus obtained from the transient state tests was lower than steady state tests due to implicit inclusion of creep in transient state tests. In order to compare the results with EN 1993-1-2 values, the results obtained with transient test methods are used to establish equations for predicting the reduction factors of yield strength, elastic modulus and proportional limit. Equations 1.a to 1.c are derived for predicting the reduction factors of yield strength at the given steel temperatures (θ):

$$\frac{f_{2.0,\theta}}{f_{0.2,20}} = 1.02 - 4\times10^{-4}\,\theta + 4.5\times10^{-7}\,\theta^2 \qquad 20\ ^\circ C \le \theta < 300\ ^\circ C \tag{1a}$$

$$\frac{f_{2.0,\theta}}{f_{0.2,20}} = 1.07 + 4\times10^{-4}\,\theta - 2.7\times10^{-6}\,\theta^2 \qquad 300\ ^\circ C \le \theta < 600\ ^\circ C \tag{1b}$$

$$\frac{f_{2.0,\theta}}{f_{0.2,20}} = 3.55 - 8.34\times10^{-3}\,\theta + 5\times10^{-6}\,\theta^2 \qquad 600\ ^\circ C \le \theta \le 800\ ^\circ C, \tag{1c}$$

where $f_{2.0,\theta}$ and $f_{0.2,20}$ are the effective yield strength at elevated temperatures and room temperature, respectively. Similarly, Equations 2.a to 2.c are derived for prediction of the reduction factors of the modulus of elasticity:

$$\frac{E_{L,\theta}}{E_{L,20}} = 1 \qquad 20^\circ C \le \theta < 200\ ^\circ C \tag{2a}$$

$$\frac{E_{L,\theta}}{E_{L,20}} = 1.14 - 6.7\times10^{-4}\,\theta \qquad 200^\circ C \le \theta < 400\ ^\circ C \tag{2b}$$

$$\frac{E_{L,\theta}}{E_{L,20}} = 7.64 - 3.26\times10^{-2}\,\theta + 4.95\times10^{-5}\,\theta^2 - 2.55\times10^{-8}\,\theta^3 \qquad 400^\circ C \le \theta \le 800\ ^\circ C, \tag{2c}$$

where $E_{L,\theta}$ and $E_{L,20}$are the moduli of elasticity at elevated temperatures and room temperature, respectively. For the prediction of the proportional limit reduction factors, Equations (3a), (3b) and (3c) are proposed:

$$\frac{f_{p,\theta}}{f_{0.2,20}} = 0.7 - 2.8\times10^{-4}\theta \qquad 20\ ^\circ C \le \theta < 300\ ^\circ C \tag{3a}$$

$$\frac{f_{p,\theta}}{f_{0.2,20}} = 1.07 - 1.5\times10^{-3}\theta \qquad 300\ ^\circ C \le \theta < 600\ ^\circ C \tag{3b}$$

$$\frac{f_{p,\theta}}{f_{0.2,20}} = 0.5 - 5.5\times10^{-4}\theta \qquad 600\ ^\circ C \le \theta \le 800\ ^\circ C, \tag{3c}$$

where $f_{p,\theta}$ is the proportional limit at elevated temperature.

The reduction factors predicted using the equations derived above are respectively presented in Figs. 15, 17, and 18(b). These figures confirm that the reduction factors predicted by the proposed equations fit well with the distribution of the reduction factors from the current tests. The results predicted by the equations also fall within the distribution of the reduction factors collected from the literature for S700 HSSs. For comparison, Figs. 15 and 17 also include the results predicted using Maraveas eq1 from Ref. [16]. The equation in Ref. [16] is derived using the whole spectrum of HSS, including strengths higher than 700 N/mm^2. It can be seen from these figures that the equations proposed in this study for yield strength and elastic modulus do not contradict those presented in the literature.

When compared to the values provided in EN 1993-1-2, reduction factors for the effective yield strength predicted by these equations is lower, while the values for elastic modulus in this study are generally higher except at 500 °C. Further comparisons show that the values for the yield strength collected from the literature are typically lower than those presented in EN 1993-1-2 between 200 °C and 400 °C. Compared

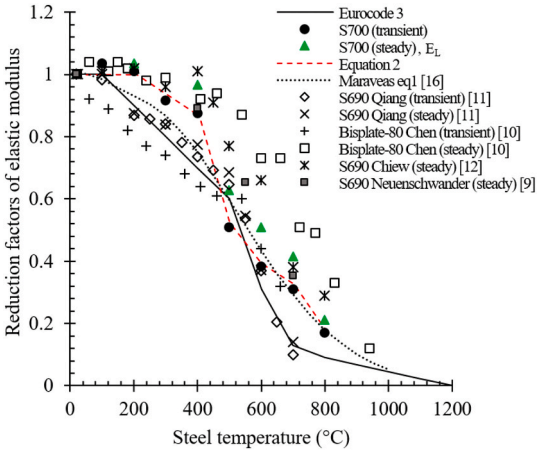

Fig. 17. Comparison of the elastic modulus reduction factors of HSS.

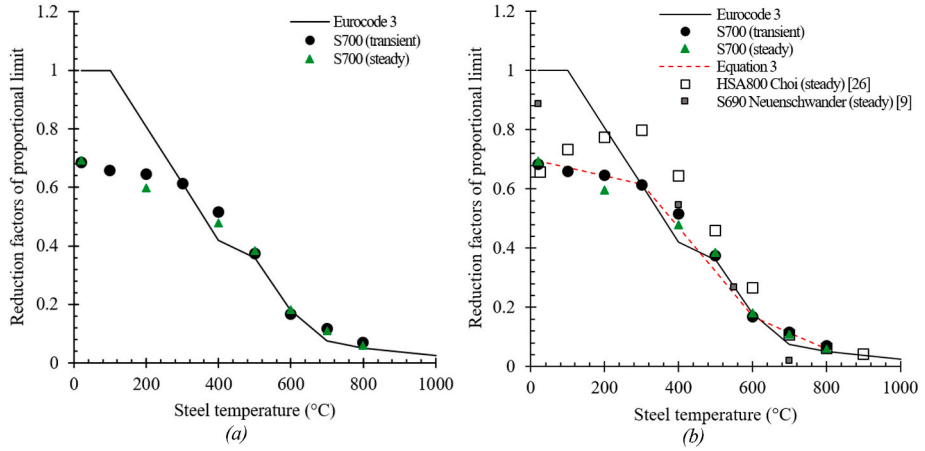

Fig. 18. Proportional limit reduction factors obtained using steady and transient state tests: (a) comparison with Eurocode 3 values; and (b) comparison with the literature values.

to yield strength reduction factors, the reduction factors of elastic modulus collected from the literature show a higher scatter and larger deviation from the values provided in EN 1993-1-2, especially above 400 °C. The dispersions indicate that HSSs, in addition to strength, should also be classified according to chemical composition and manufacturing process when defining their mechanical properties at elevated temperatures. In order to obtain reliable equations, it is necessary to perform more tests and collect more data on HSSs with different chemical compositions and manufacturing processes. The reduction factors for yield strength of HSS given in EN 1993-1-2 should be revised, especially between 200 °C and 400 °C, and the reduction factors for the modulus of elasticity should be revised for the whole temperature range. In order to establish the predictive equations for material modelling, it is recommended that the equations for HSSs should also be validated by testing structural members.

4.3. Material modelling using measured mechanical properties

In this section, the applicability of the material model in EN 1993-1-2 for the tested steel is studied. In Fig. 19(a) and (b), the curves of transient state and steady state tests are compared with the material model curves obtained from the stress-strain formulations and the reduction factors provided in EN 1993-1-2. Except at 20 °C, stress-strain curves of the tests are lower than those predicted using the material model of EN 1993-1-2. Therefore, the stress-strain curves in EN 1993-1-2 are used by replacing the reduction factors provided in EN 1993-1-2 with the corresponding values obtained from the tests. The comparisons of the stress-strain curves of the material model after this modification with the curves of the transient and steady state tests are shown in Fig. 20(a) and (b), respectively.

Fig. 20(a) shows that, up to the strain limit of 4%, the curves predicted using the reduction factors determined using Equations (1a), (1b) and (1c) fit the test results reasonably. However, some differences in the transition curve portion at the temperatures of 20 °C and 600 °C can be observed. The difference at 20 °C is due to the reduction factor of proportional limit being defined differently in this study versus EN 1993-1-2. The difference at 600 °C seems to be due to the scatter of the test results.

In Fig. 20(b), the reduction factors from steady state tests are used to obtain the stress-strain curves by modifying the material model in EN 1993-1-2. For 20 °C and 200 °C, the test curves continue to rise after 2% strain due to strain hardening. For other temperatures, the curves show no strain hardening; instead, the stress-strain curves drop at around 5% strain. In addition, a mismatch with the ultimate uniform strains and strains at fracture can be observed between tested and predicted values. Therefore, further comprehensive measurement of these strain values is recommended to get these strain limits. In addition, it can be seen from the figure that the transition portion of the stress-strain curves is not predicted well by the EN 1993-1-2 material model. Therefore, for steady state tests, a new set of equations are proposed based on Ramberg-Osgood formulations, which have been used for material modelling of steel at elevated temperatures in Refs. [23,27].

Based on the derivation in the Annex, the stress (σ) and strain (ε) relation at the steel temperature of θ can be defined by

$$\varepsilon_\theta = \frac{\sigma_\theta}{E_\theta} + \beta_\theta . \frac{f_{y,\theta}}{E_\theta} . \left(\frac{\sigma_\theta}{f_{y,\theta}}\right)^{n_\theta} , \tag{4a}$$

where β_θ and n_θ represent the degrees of non-linearity and hardening of the stress-strain curve, respectively. Using the effective yield strength at the strain of 2% $(f_{2.\theta})$ and the modulus of elasticity (E_θ) at the temperature of θ, the values of β_θ are defined by

$$\beta_\theta = 0.02 \frac{E_\theta}{f_{2.\theta}} - 1 \tag{4b}$$

The hardening parameter n_θ can be determined by fitting the material model curves with the curves obtained from the tests at different temperatures. The values of β_θ and n_θ are presented in Table 8.

Based on the values listed in Table 8, the following equations are proposed to determine the hardening factor of n_θ:

$$n_\theta = 32 - 0.115\,\theta + 4 \times 10^{-4}\,\theta^2 \qquad 20\ ^\circ C \le \theta < 400\ ^\circ C \tag{5a}$$

$$n_\theta = 50 \qquad 400\ ^\circ C \le \theta \le 800\ ^\circ C. \tag{5b}$$

The stress-strain curves predicted using Equations (4a) and (4b), (5a) and (5b) at various temperatures are presented in Fig. 21 and are compared with the curves from steady state tests. The comparison shows that the material model and the test results match reasonably from a practical point of view. The hardening behaviour of the curves at 20 °C and 200 °C is captured well by the material model. For the remaining temperatures, hardening has not been observed in the curves obtained from the tests; instead, the stress gradually starts dropping at 5% strain level. Therefore, the stress is considered constant after the strain of 2% for the prediction, and the stress-strain curves are presented up to the strain of 10%.

5. Summary and conclusions

Mechanical properties for S700 MC steel (up to 800 °C) were presented based on the results obtained from both transient state and steady state tests. The reduction factors for the mechanical properties were determined and compared with those presented in the design code of EN 1993-1-2. While the effective yield strength in EN 1993-1-2 has no reduction up to temperatures of 400 °C, the values from the test results indicated reduction from 100 °C onwards being consistently below the code values for most of the temperature range. For the proportional

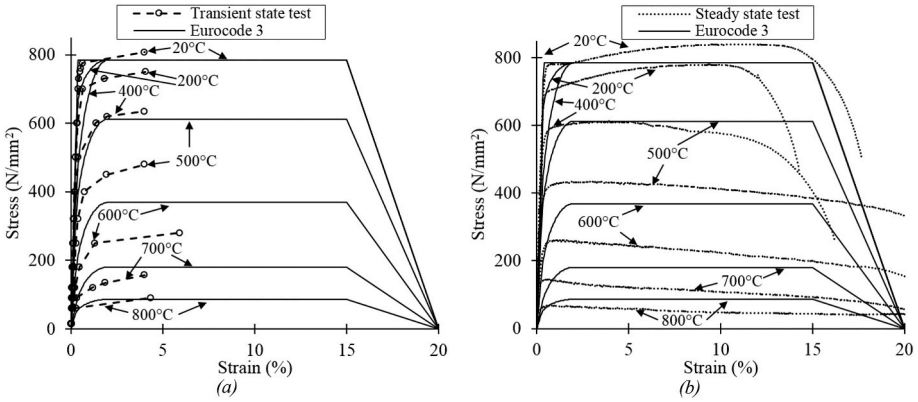

Fig. 19. Comparison of the material model curves obtained from EN 1993-1-2 formulations with (a) transient state tests, and (b) steady state tests.

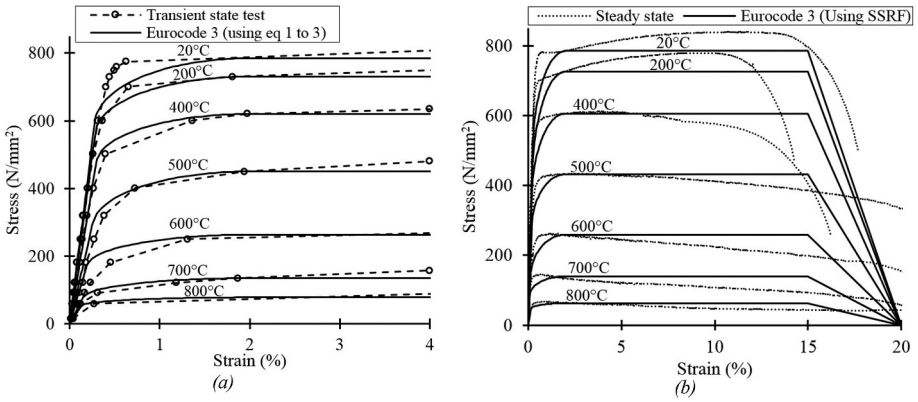

Fig. 20. Comparison of the material model curves obtained from EN 1993-1-2 formulations with (a) results from transient state tests up to 4% strain level, and (b) results from steady-state tests at full range of strains. (SSRF: steady state reduction factor).

Table 8
Values of material model curve parameters with respect to temperature.

Temperature (°C)	20	200	400	500	600	700	800
β_θ	4.50	5.11	5.82	5.23	7.56	11.82	13.24
n_θ	30	25	50	50	50	50	50

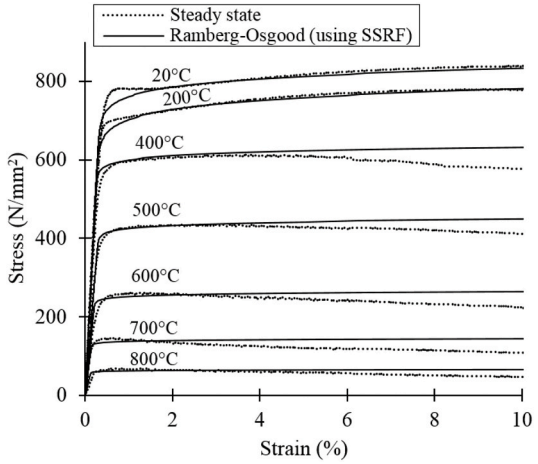

Fig. 21. Comparison of the stress-strain curves from steady state tests with the curves from Ramberg-Osgood formulation (SSRF: steady state reduction factor).

limit, test results at room temperature were below effective yield limit leading to reduction factors clearly smaller than the code values up to temperatures of 200 °C. For the modulus of elasticity, the reduction factors obtained in this study were in general larger than the code values. In this research, the modulus of elasticity was measured with both monotonic and repeated loading tests. The resulting values were consistent for lower temperatures but were relatively more dispersed above 400 °C. This dispersion can be attributed to increasing hysteresis behaviour and the microstructural changes of the steel when the temperatures are high, and the initial linear portion of the stress-strain curves is short or non-existing.

The reduction factors obtained in this study and those presented in the literature showed a larger dispersion for the elastic modulus than for the yield strength. The modulus of elasticity is usually defined using the initial linear portion of the stress-strain curves. However, in addition to the non-linear material behaviour at elevated temperatures, the test methods, the choice of procedures for data fitting and the noise in the data can further contribute to this dispersion. In order to obtain reliable results, it is recommended to perform more tests on HSSs considering different chemical compositions and manufacturing processes.

Equations for calculating the reduction factors for the mechanical properties of S700 MC were proposed based on the results of the transient state tests. These equations were used with the material model provided in EN 1993-1-2 to produce stress-strain curves that showed good agreement with the curves obtained from the transient state tests. In order to apply these equations to material modelling for practical applications, further validation by testing structural members is recommended.

As for the results obtained from the steady state tests, based on Ramberg-Osgood model, another set of equations was also proposed. The comparison between the curves obtained from two types of tests and the curves derived from their respective material models show that the models using the proposed parameters represent the material behaviour well. Another important observation is that the ultimate strains and strains at fracture in the stress-strain curves of the tests do not match with the curves of the material model provided in the current EN1993-1-2. Therefore, further studies are recommended to accommodate these strain limits in material modelling.

CRediT authorship contribution statement

Saani Shakil: Conceptualization, Data curation, Investigation, Writing - original draft. **Wei Lu:** Conceptualization, Methodology, Supervision, Writing - review & editing. **Jari Puttonen:** Supervision, Conceptualization, Writing - review & editing.

Declaration of competing interest

The authors declare that they have no known competing financial interests or personal relationships that could have appeared to influence the work reported in this paper.

Acknowledgements

The authors would like to acknowledge the *Academy of Finland* for supporting the current research (Project no. 289037). Our gratitude is further extended to Ruukki Construction Oy, Finland for providing us with the steel material. The authors are also grateful for the help of the laboratory personnel of the Department of Civil Engineering.

Annex. Derivation of stress-strain relation based on Ramberg and Osgood equation

At room temperature, the stress-strain curve can be expressed as

$$\varepsilon = \varepsilon_{el} + \varepsilon_{pl} = \frac{\sigma}{E} + \left(\frac{\sigma}{B}\right)^n \tag{4}$$

where ε and σ are the strain and stress, $\varepsilon_{el} = \sigma/E$ is the elastic strain, $\varepsilon_{pl} = \left(\frac{\sigma}{B}\right)^n$ is the plastic strain, E is the modulus of the elasticity, and B and n are material dependent constants. The stress-strain curve can be normalized by the selected values of base stress, σ_0, and base strain, ε_0. Ramberg and Osgood [28] used the secant yield stress to define the base stress. By selecting the secant modulus of elasticity as $E_{sec} = 0.7E$, the base stress has a similar value to that obtained by the 0.2% offset method. The base strain is then calculated as $\varepsilon_0 = \sigma_0/E_0 = \sigma_0/E$, with $E_0 = E$ being the base modulus of elasticity. The meaning of the base stress and the base strain is shown in Fig. 1(a).

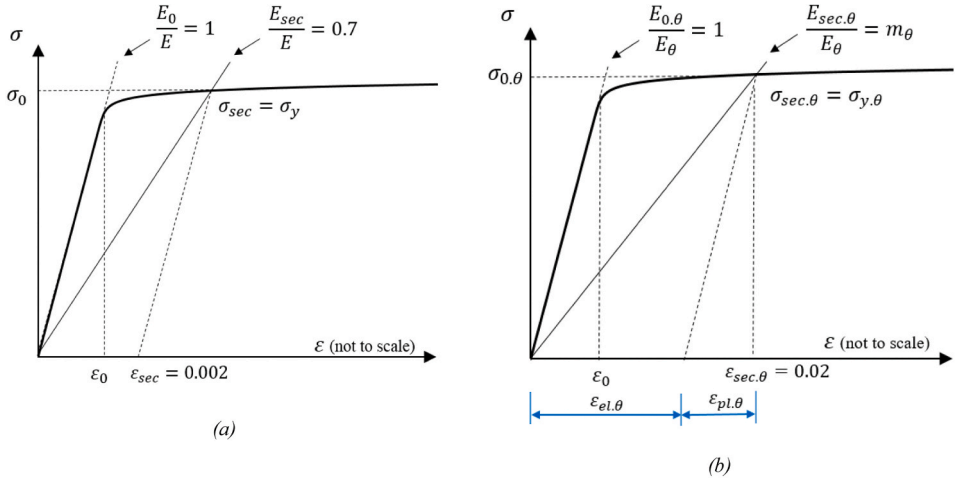

Fig. 1. Definition of base stress and base strain based on Ramberg and Osgood relation (a) at room temperature and (b) at elevated temperature.

Following this method but integrating the temperature effect into the material properties, Equation (4) can be modified as.

$$\frac{\varepsilon_\theta}{\varepsilon_{0.\theta}} = \frac{\sigma_\theta}{E_\theta \varepsilon_{0.\theta}} + \frac{1}{\varepsilon_{0.\theta}}\left(\frac{\sigma_\theta}{B_\theta}\right)^{n_\theta} = \frac{\sigma_\theta}{\sigma_{0.\theta}} + \frac{E_\theta}{\sigma_{0.\theta}}\left(\frac{\sigma_\theta}{B_\theta}\right)^{n_\theta}, \tag{5}$$

where the corresponding parameter has the same meaning as defined previously but at temperature θ. Equation (5) can be further reorganized as

$$\frac{\varepsilon_\theta}{\varepsilon_{0.\theta}} = \frac{\sigma_\theta}{\sigma_{0.\theta}} + \frac{E_\theta}{B_\theta^{n_\theta}}\frac{\sigma_\theta^{n_\theta}}{\sigma_{0.\theta}}, \tag{6}$$

The ratio of $\frac{E_\theta}{B_\theta^{n_\theta}}$ can be determined by the secant modulus of elasticity and the secant yield stress, $\sigma_{sec.\theta}$. As shown in Fig. 1(b), the secant strain at temperature θ can be expressed as:

$$\varepsilon_{sec.\theta} = \varepsilon_{el.\theta} + \varepsilon_{pl.\theta} = \frac{\sigma_{sec.\theta}}{E_\theta} + \left(\frac{\sigma_{sec.\theta}}{B}\right)^n, \tag{7}$$

The secant strain can be denoted by the secant modulus of elasticity as

$$\varepsilon_{sec.\theta} = \frac{\sigma_{sec.\theta}}{E_{sec.\theta}} = \frac{\sigma_{sec.\theta}}{m_\theta \cdot E_\theta}, \tag{8}$$

where m_θ is the ratio between $E_{sec.\theta}$ and E_θ at temperature θ. By substituting Equation (7) into Equation (6), the ratio of $\frac{E_\theta}{B_\theta^{n_\theta}}$ can be obtained as

$$\frac{E_\theta}{B_\theta^{n_\theta}} = \frac{1 - m_\theta}{m_\theta} \cdot \sigma_{sec.\theta}^{\,1-n} \tag{9}$$

By substituting Equation (8) into Equation (5) and defining $\sigma_{sec.\theta} = \sigma_{0.\theta}$, the following equation can be obtained.

$$\varepsilon_\theta = \frac{\sigma_\theta}{E_\theta} + \frac{1 - m_\theta}{m_\theta} \cdot \frac{\sigma_{0.\theta}}{E_\theta} \cdot \left(\frac{\sigma_\theta}{\sigma_{0.\theta}}\right)^{n_\theta} \tag{10}$$

In EN 1993-1-2, the effective yield stress is defined as the stress at a strain of 0.02. If setting the effective yield stress as the base stress, i.e., $\sigma_{0.\theta} = f_{2.\theta}$, then the secant modulus of elasticity can be expressed as Equation (11)

$$m_\theta = \frac{E_{sec.\theta}}{E_\theta} = \frac{\sigma_{sec.\theta}}{\varepsilon_{sec.\theta}} \cdot \frac{1}{E_\theta} = \frac{f_{2.\theta}}{0.02} \cdot \frac{1}{E_\theta} = 50\frac{f_{2.\theta}}{E_\theta} \tag{11}$$

By substituting Equation (10) into Equation (9), the strain Equation (12) at temperature θ can be determined as

$$\varepsilon_\theta = \frac{\sigma_\theta}{E_\theta} + \left(0.02\frac{E_\theta}{f_{2.\theta}} - 1\right)\cdot\frac{f_{2.\theta}}{E_\theta}\cdot\left(\frac{\sigma_\theta}{f_{2.\theta}}\right)^{n_\theta} \quad (12)$$

The value of hardening factor (n_θ) can be obtained by curve fitting with the test results.

References

[1] The Steel Construction Institute, "Investigation of Broadgate Phase 8 Fire", Structural Fire Engineering, 1991. England.
[2] T.P. McAllister, Structural Fire Response and Probable Collapse Sequence of World Trade Center Building 7, Federal Building and Fire Safety Investigation of the World Trade Center Disaster (NIST NCSTAR 1-9) Volumes 1 and 2, National Institute of Standards and Technology, 2008.
[3] L. Lu, G. Yuan, Z. Huang, Q. Shu, Q. Li, Performance-based analysis of large steel truss roof structure in fire, Fire Saf. J. 93 (2017) 21–38.
[4] A. Law, The role of modelling in structural fire engineering design, Fire Saf. J. 80 (2016) 89–94.
[5] X. Dai, S. Welch, A. Usmani, A critical review of ''travelling fire'' scenarios for performance-based structural engineering, Fire Saf. J. 91 (2017) 568–578.
[6] J. Outinen, P. Tojakander, W. Lu, J. Puttonen, Material properties of high strength steel in fire, in: Eurosteel 2014, Naples, 2014.
[7] W. Wang, L. Zhang, Mechanical properties of high strength Q690 steel at elevated temperatures, in: Eurosteel 2017, Copenhagen, 2017.
[8] Y. Du, J.R. Liew, M.-X. Xiong, Effects of heat-treatment methods on mechanical performance of high-tensile strength steel subject to elevated temperatures, in: Eurosteel 2017, Copenhagen, 2017.
[9] M. Neuenschwander, C. Scandella, M. Knobloch, M. Fontana, Modeling elevated-temperature mechanical behavior of high and ultra-high strength steels in structural fire design, Mater. Des. 136 (2017) 81–102.
[10] J. Chen, B. Young, B. Uy, Behavior of high strength structural steel at elevated temperatures, J. Struct. Eng. 132 (12) (2006) 1948–1954.
[11] X. Qiang, F. Bijlaard, H. Kolstein, Dependence of mechanical properties of high strength steel S690 on elevated temperatures, Construct. Build. Mater. 30 (2012) 73–79.
[12] S. Chiew, M. Zhao, C. Lee, Mechanical properties of heat-treated high strength steel under fire/post-fire conditions, J. Constr. Steel Res. 98 (2014) 12–19.
[13] D.A. Winful, K.A. Cashell, S. Afshan, A.M. Barnes, R.J. Pargeter, Material properties of high strength steel under fire conditions, in: Eurosteel, Copenhagen, 2017.
[14] J. Jiang, W. Bao, Z. Peng, Y. Wang, J. Liu, X. Dai, Experimental investigation on mechanical behaviours of TMCP high strength steel, Construct. Build. Mater. 200 (2019) 664–680.
[15] EN 1993-1-2, "Design of Steel Structures - Part 1-2: General Rules - Structural Fire Design, *CEN*, Brussels, 2005.
[16] C. Maraveas, Z.C. Fasoulakis, K.D. Tsavdaridis, Mechanical properties of high and very high steel at elevated temperatures and after cooling down, Fire Sci. Rev. 6 (3) (2017) 1–13.
[17] S. Shakil, W. Lu, J. Puttonen, Response of high-strength steel beam and single-storey frame in fire: numerical simulation, J. Constr. Steel Res. 148 (2018) 551–561.
[18] EN 10051, Continuously Hot-Rolled Strip and Plate/sheet Cut from Wide Strip of Non-alloy and Alloy Steels - Tolerances on Dimensions and Shapes, CEN, Brussels, 2010.
[19] EN 10149-2, Hot Rolled Flat Products Made of High Yield Strength Steels for Cold Forming-Part 2: Technical Delivery Conditions for Thermomechanically Rolled Steels, CEN, Brussels, 2013.
[20] EN ISO 6892-2, Metallic Materials. Tensile Testing. Part 2: Method of Test at Elevated Temperature, 2011.
[21] N. Toric, R.R. Sun, I.W. Burgess, Creep-free fire analysis of steel structures with Eurocode 3 material model, J. Struct. Fire Eng. 7 (3) (2016) 234–248.
[22] EN ISO 6892-1, Metallic Materials. Tensile Testing. Part 1: Method of Test at Room Temperature, 2009.
[23] T. Ranawaka, M. Mahendran, Experimental study of the mechanical properties of light gauge cold-formed steels at elevated temperatures, Fire Saf. J. 44 (2) (2009) 219–229.
[24] A. Rubert, P. Schaumann, Structural steel and plane frame assemblies under fire action, Fire Saf. J. 10 (3) (1986) 173–184.
[25] G.Q. Li, L. Huang, C. Zhang, Experimental study on high temperature elastic modulus of China made high strength structural steel, in: Eurosteel 2017, Copenhagen, 2017.
[26] I.R. Choi, K.S. Chung, D.H. Kim, Thermal and mechanical properties of high-strength structural steel HSA800 at elevated temperatures, Mater. Des. 63 (2014) 544–551.
[27] J. Outinen, Mechanical Properties of Steel Structures at Elevated Temperatures, Licentiate Thesis, Helsinki University of Technology, Finland, 1999.
[28] W. Ramberg, W.R. Osgood, Description of Stress-Strain Curves by Three Parameters, NACA Technical Note No. 902, 1943.